DOI: 10.1002/chem.200701282

High-Energy X-ray Absorption Spectroscopy: A New Tool for Structural Investigations of Lanthanoids and Third-Row Transition Elements

Paola D'Angelo,*[a] Simone De Panfilis,[b] Adriano Filipponi,[c] and Ingmar Persson[d]

Abstract: This is the first systematic study exploring the potential of high-energy EXAFS as a structural tool for lanthanoids and third-row transition elements. The K-edge X-ray absorption spectra of the hydrated lanthanoid(III) ions both in aqueous solution and in solid trifluoromethanesulfonate salts have been studied. The K-edges of lanthanoids cover the energy range from 38 (La) to 65 keV (Lu), while the corresponding energy range for the L_3-edges is 5.5 (La) to 9.2 keV (Lu). We show that the large widths of the core-hole states do not appreciably reduce the potential structural information in the high-energy K-edge EXAFS data. Moreover, for lanthanoid compounds, more accurate structural parameters are obtained from analysis of K-edge than from L_3-edge EXAFS data. The main reasons are the much wider k range available and the absence of double-electron transitions, especially for the lighter lanthanoids. A comparative K- and L_3-edge EXAFS data analysis of nonahydrated crystalline neodymium(III) trifluoromethanesulfonate demonstrates the clear advantages of K-edge analysis over conventionally performed studies at the L_3-absorption edge for structural investigations of lanthanoid and third-row transition metal compounds. The coordination chemistry of the hydrated lanthanoid(III) ions in aqueous solution and solid trifluoromethanesulfonate salts, based on the results of both the K- and L_3-edge EXAFS data, is thoroughly discussed in the next paper in this series (I. Persson, P. D'Angelo, S. De Panfilis, M. Sandström, L. Eriksson, *Chem. Eur. J.* **2008**, *14*, DOI: 10.1002/chem.200701281).

Keywords: EXAFS spectroscopy · hydrates · lanthanides · solution structures · X-ray absorption spectroscopy

Introduction

X-ray absorption spectroscopy (XAS) is an excellent tool for investigating the coordination structure of electrolyte solutions. The major advantages of XAS over diffraction techniques are its sensitivity to short-range order and site selectivity, which make this method a unique probe for structural determination of the first coordination shell of metal complexes in electrolyte solutions. A major weakness in EXAFS studies on lanthanoid compounds using the L_3-edge (5483 eV for La) is the short data range, due to the appearance of the L_2-edge (5891 eV for La). This limits the effective k range for EXAFS studies to less than 400 eV for La and thus considerably decreases the resolution. Furthermore, L_3-edge EXAFS spectra of lighter lanthanoid(III) compounds show a couple of very intense features in the k range of 5–7 $Å^{-1}$, which have been assigned to double-electron transitions $2p4d \rightarrow 5d^2$.[1,2] It is well known that double-electron excitations modify the fine structure beyond the absorption edge and introduce errors in the determination of bond length and coordination number, and the effect is proportional to the magnitude of the double-excitation peak.[3]

In this context, XAS spectra above the K-edge of lanthanoids(III) could be used to address some of the aforementioned shortcomings. In general EXAFS has been confined to absorption edges below 30 keV, as the structural signal can be strongly damped at very high energy. In fact, the higher the energy of the absorption edge, the shorter the lifetime of the excited atomic state, and the greater the damping and broadening of the signal. This affects in partic-

[a] Prof. P. D'Angelo
Dipartimento di Chimica, Università di Roma "La Sapienza"
P. le A. Moro 5, 00185 Roma (Italy)
E-mail: p.dangelo@caspur.it

[b] Dr. S. De Panfilis
CRS-SOFT INFM-CNR
Dipartimento di Fisica, Università di Roma "La Sapienza"
P. le A. Moro 5, 00185 Roma (Italy)

[c] Prof. A. Filipponi
Dipartimento di Fisica, Università dell' Aquila
Via Vetoio, 67010 Coppito, L' Aquila (Italy)

[d] Prof. I. Persson
Department of Chemistry
Swedish University of Agricultural Sciences
P.O. Box 7015, 75007 Uppsala (Sweden)

ular the high-frequency components of the measured signal and consequently reduces the sensitivity of the technique to the more distant coordination shells. Nevertheless, recent EXAFS investigations on solid Eu_2O_3 at the K-edge have shown that although the core-hole width is five time larger at the K-edge than at the L_3-edge, the corresponding loss of information is largely remediated by the wide k range, the extent of which is more than twice that of the L_3-edge of the lighter lanthanoids.[4] In addition, in the case of disordered systems such as aqueous solutions, high-frequency components are strongly damped in the spectra, and the structural information content of the K-edge data is the same as that of the L_3-edge data. Another important advantage of using the K-edge spectra is that at very high energy the absorption of most materials is very low, and the samples can be held in cells with almost any type of window. This facilitates, for example, the use of high-pressure cells to perform experiments under extreme conditions of pressure and temperature. Nowadays, high energies are commonly accessible from third-generation synchrotron radiation sources and beamlines that can provide sufficient flux up to 70–80 keV. In particular, previous experimental work at high energy has been performed at the BM29[4,5] and GILDA[6] beamlines of the European Synchrotron Radiation Facility (ESRF) in France, and at the SPring-8 Facility[7,8] in Japan.

The aim of the present work is to explore the potential of EXAFS spectroscopy at K-edge absorption energies higher than 38 keV. For a systematic study one needs a series of elements with varying absorption energy and, in principle, the same structure. In this context the hydrated lanthanoid(III) ions are an ideal set of probes, as they contain fourteen elements with very similar chemical properties and very small systematic changes in their structures. Here the data analysis of solid isostructural nonaaqualanthanoid(III) trifluoromethanesulfonates $[Ln(H_2O)_9](CF_3SO_3)_3$ is presented. The lanthanoid(III) ions have furthermore been shown to have almost identical structures both in the solid state and solution.[9] We present a complete data set for both solids and aqueous solutions at both K- and L_3-edges, which allows direct comparison to be made. The presentation of the detailed coordination chemistry of these systems is made in the adjacent paper.[9] Similar studies have also been performed on dimethyl sulfoxide-solvated lanthanoid(III) ions in solid iodide salts and in solution, all of which are eight-coordinate in a square-antiprismatic fashion,[10] and on *N*,*N*′-dimethylpropyleneurea-solvated lanthanoid(III) ions in solid iodide salts and in solution,[11] where the lanthanoids are six- and seven-coordinate, respectively. Here, we present a detailed description of the data treatment only for two examples, neodymium and lutetium, as they have large differences in absorption energy. Moreover, we intend to provide with this study, and with the separate investigations on the series of hydrated and solvated lanthanoid(III) ions reported in the following paper in this series,[9] a reference work for future application to other systems containing elements absorbing X-rays at energies above 30 keV. This work should stimulate others to perform high-energy EXAFS studies, as it has several advantages over low-energy L_3-edge EXAFS.

Results

High-energy K-edge X-ray absorption spectra: In condensed systems the X-ray absorption cross section is characterized by well-defined absorption edges corresponding to the onset of core-electron excitations to unoccupied electronic levels, and sharp features due to transitions to discrete resonances. The edge features are broadened by intrinsic and instrumental effects, the former of which are essentially determined by the finite lifetime of the excited atomic state. Figure 1 A shows the K-edge X-ray absorption near-edge structure (XANES) spectra of lanthanoid(III) ions in aqueous solution, where the effect of the core-hole lifetime on high-energy spectra is clearly visible.

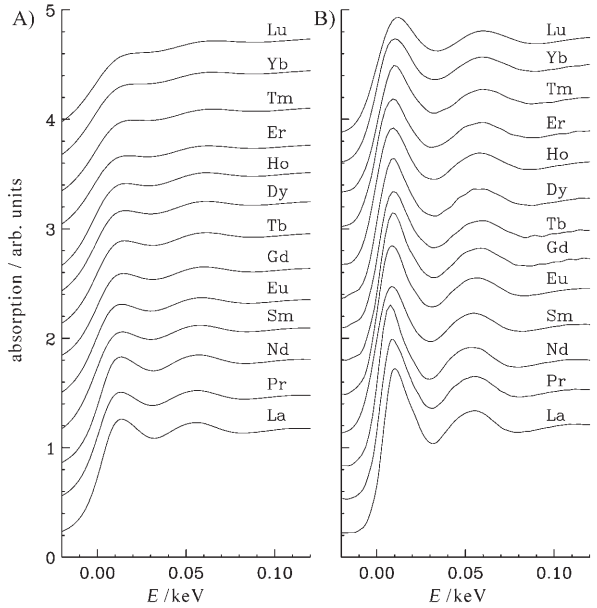

Figure 1. A) Normalized K-edge X-ray absorption spectra of lanthanoid(III) ions in aqueous solution. The zero positions correspond to the first inflection point of each spectrum. B) K-edge X-ray absorption spectra of lanthanoid(III) ions in aqueous solution after deconvolution of the core-hole widths.

As expected, the edge resonance is strongly damped and the intensity of the main transition peaks becomes much smaller on going from lanthanum(III) to lutetium(III). The core-hole widths at the K-edge are $\Gamma = 14.1$ and 33.7 eV for lanthanum and lutetium, respectively.[12]

The EXAFS spectra of the hydrated lanthanoid(III) ions in aqueous solution above the K-edge are reported in Figure 2. Despite the extremely large core-hole widths, the structural signals are detectable with good signal-to-noise ratio up to 13 $Å^{-1}$. The frequencies of the EXAFS oscillations reveal a structural trend across the lanthanoid(III) series. In particular, contraction of the lanthanoid(III)–

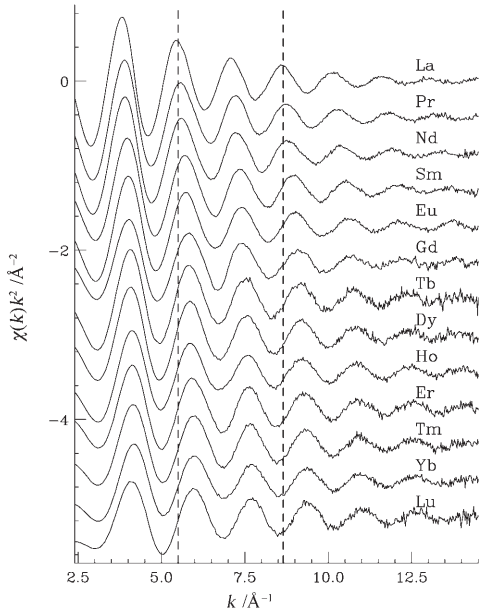

Figure 2. K-edge EXAFS spectra of lanthanoid(III) ions in aqueous solution.

oxygen first-shell distance occurs on going from lanthanum(III) to lutetium(III) as a result of the decreasing ionic radii throughout the series due to the lanthanoid contraction.

As the core-hole effect provides a constant broadening in energy space, the low-k region of the XAS spectra is more affected than the higher k region. Moreover, when dealing with K-edge spectra at very high energies, the influence of the Debye–Waller (DW) term is stronger than normally encountered at lower energies, and this makes it impossible to detect more distant shells when working at room temperature. The effect of the core-hole width on the low-k range is clearly detectable in the spectra of hydrated lanthanoid(III) ions, especially for elements of higher atomic number, but the damping is not as dramatic as in the case of solid samples such as platinum[7] or Eu_2O_3.[4] In disordered systems, such as aqueous solutions, due to the broad correlation functions at large distances the medium-range order only weakly affects the absorption spectra, and EXAFS is essentially insensitive to the higher coordination shells. Therefore, the structural information that can be extracted from the high-energy EXAFS spectra at the K-edge is the same, if not more complete, as that of the L_3-edge.

Since multiple-scattering effects make large contributions to the low-energy range of the absorption spectra, XANES is very sensitive to the geometric environment of the absorbing site. Therefore, its quantitative analysis may provide additional insights into the coordination structure of the photoabsorber atom which are not achievable from analysis of the EXAFS region. As previously shown, XANES spectra at very high energies are strongly broadened by the core-hole widths and the structural oscillations are smeared out in the spectra. Recently, it was suggested to deconvolute the core-hole width in the analysis of X-ray absorption spectra.[13] This treatment greatly facilitates the detection of spectral features and comparison with theoretical calculations. Figure 1 B shows the X-ray absorption spectra of lanthanoid(III) ions in aqueous solution for which deconvolution of the tabulated core-hole widths has been performed, by applying Gaussian filters with full widths at half-maximum ranging from 2.8 to 7.5 eV. The trend of the white-line intensity observed in Figure 1 B is mainly related to the Gaussian filter used in the deconvolution procedure, and no physical information can be derived from it. An ideal deconvolution with no filter would provide the real shape of the XANES region, but due to the finite noise level of the experimental data, this approach is actually impossible. After deconvolution, the threshold regions are considerably sharpened with respect to the original spectra, and the intensity of the structural oscillations is also clearly enhanced. To test the reliability of this procedure, the deconvoluted K-edge spectrum of neodymium(III) in aqueous solution is compared with the L_1 spectrum in Figure 3 A.

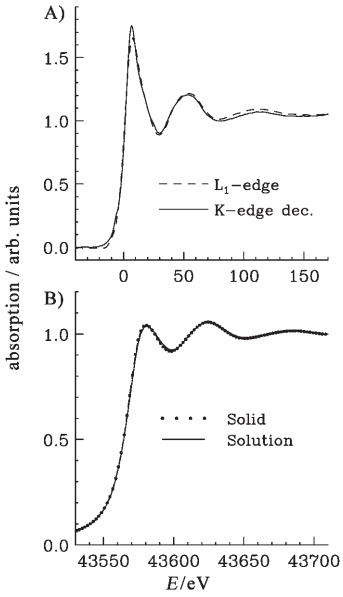

Figure 3. A) Comparison between L_1-edge (dashed line) and deconvoluted K-edge (solid line) XANES spectra of $[Nd(H_2O)_9]^{3+}$ in aqueous solution. B) Comparison between the K-edge XANES spectra of $[Nd(H_2O)_9]^{3+}$ in aqueous solution (solid line) and solid $[Nd(H_2O)_9](CF_3SO_3)_3$ (dotted line).

Note that the two spectra have similar shapes since the broadening associated with the core-hole width of the L_1-edge ($\Gamma = 4.52$ eV), which has not been removed, is comparable with that in the deconvoluted K-edge spectrum due to the adopted Gaussian filter with $\sigma = 4.5$ eV and additional resolution broadening by the monochromator. The similarity of the two spectra demonstrates that deconvolution of the core-hole width in high-quality, low-noise K-edge spectra can reveal most of the structural and electronic information they contain. Thus, one can use the XANES spectra at the K-edge to obtain structural and electronic information on systems absorbing at very high energies of 40 keV or more.

This is an advantage, as the theoretical framework for quantitative analysis of the XANES at K-edges is less problematic and better established.

Multielectron excitations: Several XAS investigations on the lanthanoid(III) and yttrium(III) ions have shown the presence of multielectron excitations at the L-edges of these elements.[1,2,14–19] In particular, the presence of anomalous peaks, appearing in the range from 5 to 7 $Å^{-1}$ and superimposed on the main single-frequency oscillatory signal, has been explained as due to double-electron transitions $2p4d \rightarrow 5d^2$ in the case of the L_3- and L_2-edges, and $2s4d \rightarrow 6p5d$ for the L_1 spectra.[2]

The EXAFS spectra of the hydrated neodymium(III) ion in aqueous solution at the L_3- and K-edges are compared in Figure 4, which clearly shows the phase difference of about

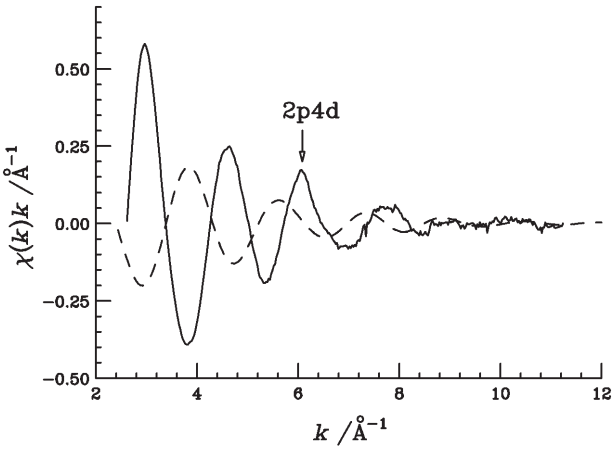

Figure 4. Comparison between the L_3-edge (solid line) and K-edge (dashed line) EXAFS spectra of $[Nd(H_2O)_9]^{3+}$ in aqueous solution. The arrow indicates the onset of the 2p4d double-electron excitation edge.

π and the higher amplitude of the L_3-edge signal. The L_3 spectrum shows an anomalous feature at about 6 $Å^{-1}$ which causes a distortion in the structural oscillation, while the K-edge spectrum contains a regular single-frequency oscillation without visible spurious peaks. As previously mentioned, recent methods of EXAFS data analysis account for the presence of double-excitation channels by properly modeling the atomic background used in the extraction of the $\chi(k)$ signal.[20] Step-shaped functions can be used to reproduce the background discontinuities and changes of slope due to the presence of double-electron transitions. Nevertheless, when the features associated with the opening of multielectron thresholds are sharp and structured, as in the case of the lanthanoid L-edges, they cannot be completely removed from the EXAFS structural oscillation. This hampers accurate determination of the structural parameters, especially for disordered systems, where the presence of multielectron transitions is more evident due to the weakness of the structural contribution.[3]

The presence of multielectron excitation channels is detected also in the K-edge spectra of aqueous solutions of the lanthanoids, but in this case they give rise to changes in slope and smooth edges in the atomic background which can be properly reproduced by the model functions used in the extraction of the EXAFS signal. The sharp features which are visible in the L_3-edge spectra are not present in the K-edge data due to the broadening effect caused by the short lifetime of the excited atomic state. In particular, of the three double-electron processes that are expected to occur in the EXAFS region, namely, the $1s4d \rightarrow 6p5d$, $1s4p \rightarrow 6p^2$, and $1s4s \rightarrow 6p7s$, only the first has appreciable intensity. This double-electron excitation can be easily included in the atomic background, and this allows extraction of the structural parameters from the experimental data with higher accuracy as compared to the L-edge spectra.

EXAFS data analysis: To assess the reliability of the XAS technique at the K-edge of lanthanoid(III) ions, here we compare K- and L_3-edge EXAFS data analysis of crystalline $[Nd(H_2O)_9](CF_3SO_3)_3$. The coordination of the neodymium(III) ion in this compound is well-established by X-ray diffraction.[21,22] Moreover, the hydrated neodymium(III) ion in aqueous solution has the same geometry as in the solid trifluoromethanesulfonate salt, as can be clearly deduced by looking at the comparative plots of the two XAS spectra in Figure 3B. In $[Nd(H_2O)_9](CF_3SO_3)_3$ the first coordination sphere is composed of nine water molecules arranged in a tricapped trigonal configuration with six prismatic and three capping Nd–O distances at 2.451 Å and 2.568 Å, respectively (see Figure 5).[21,22] In the first step the EXAFS data were analyzed with a two-shell model. Least-squares fits of the EXAFS spectra were performed in the range $k = 2.4$–16.3 $Å^{-1}$ for the K-edge, while a smaller k interval (2.8–11.3 $Å^{-1}$) was analyzed in the case of the L_3-edge. Fitting procedures were applied to the whole set of structural and nonstructural parameters to improve, as far as possible, the agreement between calculated signals and experimental spectra. In particular, we optimized four structural parameters for each single-shell contribution, and two additional structural parameters (the O-Nd-O angle and its variance) for the three-body contribution. The best-fit analyses of the L_3- and K-edge EXAFS spectra are shown in the upper panels of Figure 5. The first five curves from the top of each panel are the Nd–O and Nd–H first-shell $\gamma^{(2)}$ contributions, and the multiple-scattering (MS) signals associated with the three short-bond O1-Nd-O1 configurations. The reminder of the figure shows comparisons of the total theoretical contributions with the experimental spectra, and the resulting residuals. Overall, the fitted EXAFS spectra match the experimental data quite well, both for the L_3- and K-edge spectra. The dominant contribution to the total XAFS signals is given by the Nd–O first-shell signals, even though, due to the well-ordered structure of the water molecules around the ion, the 12 plus 6 hydrogen atoms of the first hydration shell give rise to rather strong $\gamma^{(2)}$ signals, which are detectable up to about $k = 11$ $Å^{-1}$ (see Figure 5). The contribution of the second hydration shell is negligible, while the MS paths from the O1-Nd-O1 configurations yield detectable amplitude signals in the low-k regions of the spectra.

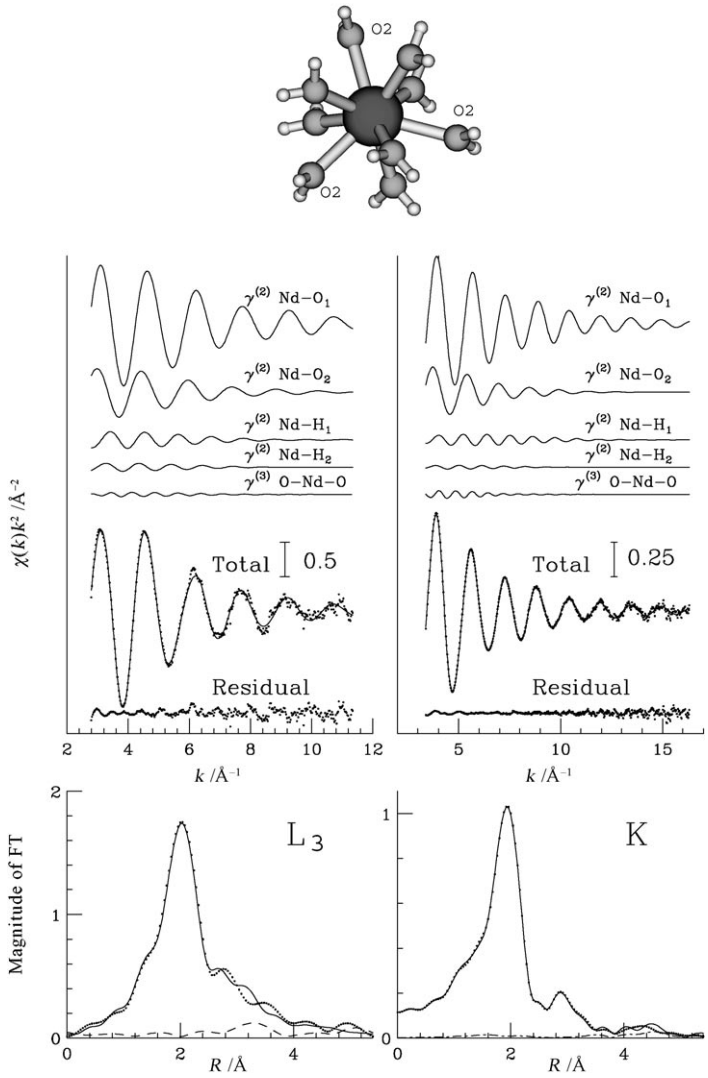

Figure 5. Fit of the L_3-edge (left panels) and K-edge (right panels) EXAFS spectra of solid neodymium(III) trifluoromethanesulfonate. From top to bottom of each panel, the following curves are reported: the Nd–O first-shell signals, the Nd–H first-shell signals, the O1-Nd-O1 three-body signal, the total theoretical signal compared with the experimental spectrum, and the residual curve. The lower panels show the Fourier transforms (not corrected for phase shift) of the experimental data (dotted line), the total theoretical signals (full line), and the residual curves (dashed-dotted line). At the top a perspective view of the first coordination shell of the hydrated neodymium(III) ion in solid $[Nd(H_2O)_9](CF_3SO_3)_3$ is shown.

As expected the signal is damped at the K-edge due to the short core-hole lifetime corresponding to a core-hole width of 17.3 eV, while a stronger signal is obtained at the L_3-edge ($\Gamma = 3.65$ eV).[12] In contrast, the presence of the L_2-edge limits the L_3-edge EXAFS spectral range to around $k = 11.8$ Å^{-1}, while reliable structural information can be extracted from the corresponding K-edge EXAFS up to $k = 16$ Å^{-1} in this case. The lower panels of Figure 5 show the corresponding k^2-weighted Fourier transform (FT) calculated with no applied phase shift correction in the k ranges of 2.8–11.3 Å^{-1} and 3.4–13.5 Å^{-1} for the L_3- and K-edge spectra, respectively. The FT spectra show a prominent first-shell peak that is mainly due to the Nd–O first-shell distances. The Nd–H first shell is located at about 2.8 Å, and is clearly separated in the K-edge signal, whilst such a separation is not possible with the L_3 real-space resolution. Longer distance contributions due to the MS paths are also visible at about 4.2 Å in the K-edge data. This example illustrates the gain in spatial resolution achieved with the large k range available when working at the K-edge in comparison with the L_3-edge. Refined values for the full set of parameters obtained from the two-shell model are listed in Table 1 for the L_3- and K-edge spectra. In both cases the Nd–O bond lengths to the six oxygen atoms in the prism and to the three capping ones are in perfect agreement with the crystallographic determination. Nevertheless, the accuracy of the structural parameters is very different between the L_3- and K-edge data. In particular, to establish error limits in the refined parameters, a statistical analysis applying two-dimensional contour plots to selected parameters of the fit was applied. This analysis examines the correlations among fitting parameters and evaluates the statistical errors by following the procedure described in detail in ref. [23]. Figure 6 shows the contour plots of the Nd–O1 and Nd–O2 distances versus E_0 for the L_3- and K-edges, where the innermost contour refers to the 95% error confidence interval. In the case of the K-edge, the error in the determination of the six Nd–O1 distances is half of that of the three Nd–O2 distances (see Table 1). This is not surprising, as in a wide radial distribution function the shorter bond lengths contribute more to the EXAFS signal than the longer ones, because of the longer period in the sinusoidal oscillations and a smaller Debye–Waller factor. This is especially true in the case of high-energy edges, as the amplitude of the high-

Table 1. First-shell structural parameters of solid neodymium(III) trifluoromethanesulfonate from the EXAFS data analysis at the K-edge and L_3-edge.[a]

	N	R [Å]	σ^2 [Å^2]	β
		K-edge		
Nd–O1	6.0(0.5)	2.495(0.009)	0.0068(0.0013)	0.5(0.1)
Nd–O2	3.0(0.8)	2.583(0.018)	0.0097(0.0045)	0.1(0.1)
Nd–H1	11.9(0.7)	3.20(0.03)	0.003(0.004)	1.4(0.5)
Nd–H2	6.0(0.8)	3.34(0.05)	0.006(0.006)	0.9(0.6)
Nd–O$_{asym}$	9.1(0.5)	2.524(0.007)	0.010(0.001)	0.7(0.1)
Nd–H$_{asym}$	18.1(0.9)	3.28(0.04)	0.011(0.003)	1.4(0.6)
Nd–O$_{Gauss}$	9.0(0.6)	2.509(0.009)	0.009(0.005)	–
Nd–H$_{Gauss}$	18.0(1.0)	3.25(0.05)	0.010(0.009)	–
		L_3-edge		
Nd–O1	6.0(1.0)	2.50(0.04)	0.014(0.006)	0.5(0.2)
Nd–O2	3.0(1.2)	2.57(0.04)	0.009(0.007)	0.1(0.3)
Nd–H1	11.9(1.0)	3.18(0.06)	0.006(0.007)	0.9(0.6)
Nd–H2	6.1(1.2)	3.28(0.08)	0.007(0.008)	0.4(0.7)
Nd–O$_{asym}$	9.0(0.8)	2.520(0.013)	0.013(0.002)	0.4(0.2)
Nd–H$_{asym}$	18.1(0.5)	2.524(0.007)	0.010(0.001)	0.5(0.6)
Nd–O$_{Gauss}$	9.0(0.7)	2.501(0.013)	0.015(0.007)	–
Nd–H$_{Gauss}$	18.0(1.2)	3.16(0.07)	0.012(0.009)	–

[a] H1/H2, O1/O2: two-shell model; asym: asymmetric single-shell model; Gauss: Gaussian single-shell model.

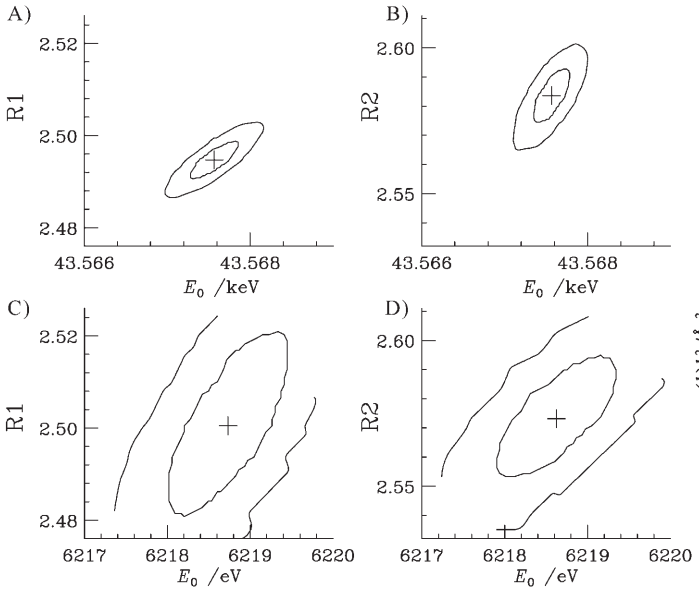

Figure 6. Two-dimensional contour plots for selected parameters in the EXAFS fit of the L_3-edge and K-edge spectra of solid nonaaquaneodymium(III) trifluoromethanesulfonate. A) R(Nd–O1) versus E_0 for the K-edge. B) R(Nd–O2) versus E_0 for the K-edge. C) R(Nd–O1) versus E_0 for the L_3-edge. D) R(Nd–O2) versus E_0 for the L_3-edge. The innermost curve of each plot corresponds to the 95% confidence interval from which the statistical errors are determined.

frequency components decreases rapidly at higher k values due to lengthening of the core-hole lifetime and the stronger Debye–Waller effect. Conversely, in the case of the L_3-edge the amplitude of the Nd–O2 $\gamma^{(2)}$ signal is comparable to that of Nd–O1 over the whole k range used in the analysis, and the error in the two distances is the same (see Table 1). The outstanding result of this analysis is that the errors in the bond lengths determined from the analysis of the K-edge data are much smaller (four and two times for the Nd–O1 and Nd–O2 distances, respectively) in comparison with the L_3-edge. This is due both to the wider k range used in the analysis of the K-edge and to the presence of strong double-electron excitations at the L_3-edge that hamper a proper extraction of the EXAFS structural signal. Note that in the case of L_3-edge the sharp peak at about 6 $Å^{-1}$ in the experimental spectrum (see Figure 5) is associated with opening of the 2p4d double-electron excitation channels. As it is not possible to mimic such a sharp peak in the extraction of the atomic background, the experimental points in a range of about 20 eV around this peak were excluded from the fitting procedure. These results demonstrate that the accuracy in the determination of the Ln^{III}–O first-shell distances is significantly higher for K-edge than for L_3-edge EXAFS data analysis. The amplitude reduction factors S_0^2 were found to be 0.99 for both edges. In addition, the positions of the theoretical energy scales were (43567.6 ± 0.5) eV and (6218.7 ± 0.5) eV for the K- and L_3-edges, respectively.

In the second step the K- and L_3-edge EXAFS spectra were analyzed with a single-shell model. Asymmetry of the positional disorder around the neodymium(III) ion was accounted for by using a gammalike distribution curve to describe the shape of the Nd–O first peak. The EXAFS data were minimized in the same k range as the previous analyses, and the results for the K-edge are shown in Figure 7A.

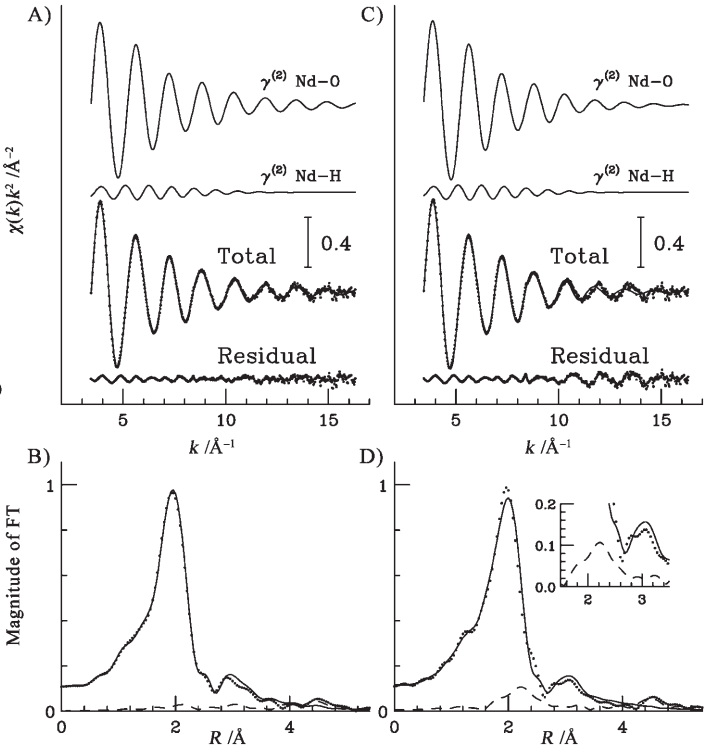

Figure 7. A) Fit of the K-edge EXAFS spectrum of solid $[Nd(H_2O)_9](CF_3SO_3)_3$ using an asymmetric single-shell model. From top to bottom the following curves are reported: the Nd–O first-shell total signal, the Nd–H first-shell total signal, the total theoretical signal compared with the experimental spectrum, and the residual curve. B) Nonphase-shift-corrected Fourier transforms of the experimental data (dotted line), of the total theoretical signals (full line), and of the residual curves (dashed-dotted line) reported in A). C) Fit of the K-edge EXAFS spectrum of solid $[Nd(H_2O)_9](CF_3SO_3)_3$ using an Gaussian single-shell model. The curves are as in A). D) Nonphase-shift-corrected Fourier transforms of the experimental data (dotted line), of the total theoretical signals (full line), and of the residual curves (dashed-dotted line) reported in C). A zoom of the region between 1.8 and 3.6 Å is shown in the inset.

In this case the first curve from the top represents the total Nd–O $\gamma^{(2)}$ theoretical signal comprising both the short and long distances of the tricapped trigonal prism, while the second curve is the theoretical signal associated with the 18 hydrogen atoms. The agreement between the experimental spectrum and the theoretical model is very good, and this is also evident from the FT spectra shown in Figure 7B. The structural parameters obtained from this analysis are reported in Table 1. Also in this case the accuracy in the determination of the Nd–O distance is higher for the K-edge than for the L_3-edge. Moreover, the error associated with the Nd–O first-shell distance is smaller than that obtained from the two-shell analysis. This is due to the large statistical correlation among the structural parameters describing the distribution of six oxygen atoms in the prism and three in cap-

ping positions, which is responsible for the large uncertainty in the refined parameters obtained from the two-shell analysis. Therefore, the structural parameters obtained from the single-shell fit are more accurate, and the gamma function allows a reliable description of the Nd–O radial distribution function. This can be verified by comparing the pair distribution functions obtained from the single- and two-shell data analyses. Figure 8A compares the Nd–O asymmetric

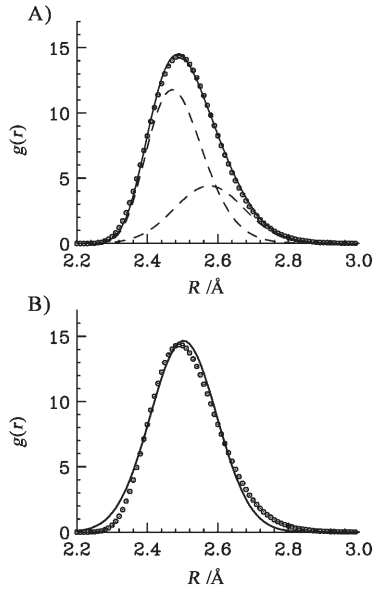

Figure 8. A) Comparison between the first-shell peak obtained from the EXAFS data analysis of the K-edge spectrum of solid $[Nd(H_2O)_9](CF_3SO_3)_3$ using a single-shell model (circles) and superposition of the Nd–O1 and Nd–O2 peaks (dashed line) obtained from the two-shell model (full line). B) Comparison between the first-shell peak obtained from the EXAFS data analysis of the K-edge spectrum of solid $[Nd(H_2O)_9](CF_3SO_3)_3$ using an asymmetric peak (circles) and a Gaussian function (full line).

peak obtained from the single-shell analysis with the superposition of the two separate Nd–O peaks. The two curves are identical, that is, the Nd–O distance distribution which is present in the tricapped trigonal structure can be properly described by using a suitable asymmetric peak.

The EXAFS data of disordered systems are often analyzed by using Gaussian peaks to model the photoabsorber coordination shell. The reliability of such an approach can be checked by comparing the results from this method with those obtained from analyses allowing asymmetric distance distributions. Curve fitting of the $\chi(k)$ signal with a Gaussian distribution (see Figure 7C) reveals a phase-shift at k values higher than 10 $Å^{-1}$, and also a displacement of the sine transform relative to the magnitude of the FT (see Figure 7D), which is an indicator of asymmetry. Note that the residual curve shows an oscillation trend for $k > 10$ $Å^{-1}$ and that the agreement between the theoretical and experimental FTs is not very good in the distance range between 1.8 and 2.8 Å. The peak at about 2.2 Å in the FT of the residual curve, which is more clearly visible in the magnified sections of the FT of Figure 7D, is clearly due to neglecting the asymmetry in the description of the neodymium(III) coordination shell.

Significant differences have been obtained in the structural parameters obtained from the Gaussian and the asymmetric peak analyses above the K-edge. In particular, the Nd–O and Nd–H Gaussian peaks are shifted towards shorter distances, while a slight decrease is observed for the Debye–Waller factors. A more direct description of the differences between the coordination-shell parameters obtained from the two EXAFS analyses can be obtained by examining the comparative plots of the refined asymmetric and Gaussian peaks shown in Figure 8B. The maximum of the Gaussian shell is shifted toward shorter distances, and the shapes of the two distributions are markedly different in both the low- and high-distance regions.

The L_3-edge is not sensitive to the asymmetry of the pair distribution. As shown in Figure 7C, the effect of the Gaussian approximation is evident in the k range above 10 $Å^{-1}$. The presence of the L_2-edge allows one to analyze the L_3 EXAFS data only up to about 11 $Å^{-1}$. As a consequence, in this case, the L-edges are not very sensitive to the shape of the oxygen distribution around the photoabsorber, and this affects the accuracy of the structural parameters obtained from the EXAFS analysis.

An important issue in the study of lanthanoid(III) ions in aqueous solution is determination of the hydration polyhedra around the lanthanoid(III) cations. To this end it is very important to establish whether the EXAFS technique is able to determine the coordination numbers with sufficient accuracy. Figure 9A and B show the contour plots for the Nd–O1 and Nd–O2 coordination numbers and Debye–Waller factors for the K- and L_3-edges, respectively. Also in this case the errors in coordination numbers determined by analysis of the L_3-edge data are higher in comparison with

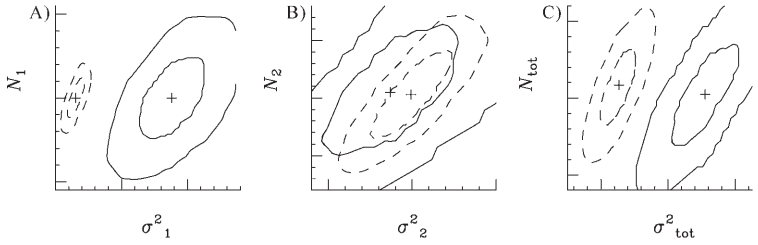

Figure 9. Two-dimensional contour plots for selected parameters in the EXAFS fit of the L_3-edge and K-edge spectra of solid $[Nd(H_2O)_9](CF_3SO_3)_3$. A) Nd–O1 coordination number versus Debye–Waller factor for the K-edge (dashed line) and for the L_3-edge (full line). B) Nd–O2 coordination number versus Debye–Waller factor for the K-edge (dashed line) and for the L_3-edge (full line). C) Nd–O total coordination number obtained from the single-shell model versus Debye–Waller factor for the K-edge (dashed line) and for the L_3-edge (full line). The innermost curve of each plot corresponds to the 95% confidence interval from which the statistical errors are determined.

the K-edge. In the case of the two-shell model there is strong statistical correlation between the amplitude parameters of the two shells, and this is reflected in the very high errors obtained form the analysis. This effect is also responsible for the quite different DW values obtained from the K- and L_3-edge data analyses. When an asymmetric single-shell model is used in the analysis of the EXAFS data, the error in the total coordination numbers becomes smaller (see Figure 9C). Nevertheless, the results of this analysis show that the uncertainty in the coordination numbers is too large for conclusive determination of the geometry of lanthanoid complexes. As a consequence, for structural studies on aqua ions in solution, the mean metal–oxygen bond length obtained from the EXAFS analysis is a more reliable indicator of the coordination number than direct determination of the number of coordinated ligands. This shows the importance of comparing the EXAFS spectra of hydrated lanthanoid(III) ions in both aqueous solution and the solid state, if the solid-state structure is well defined and well determined. Furthermore, different configurations will give somewhat different multiple scattering patterns even when the M–O bond lengths are fairly similar. Therefore, identical EXAFS spectra of a species in solid state and aqueous solution show that the structure in the solid state is maintained in solution.

The hydrogen contribution: Previous work on 3d transition metal ions in aqueous solution showed that the EXAFS technique can provide reliable structural information on the ion–H pair distribution function $g(r)$ of ionic solutions.[24] Neutron diffraction (ND) is the only alternative experimental technique which can give information on the ion–H $g(r)$; provided the ion–O first-shell distance is known, the orientation distribution of the hydrated water molecules can be obtained by ND. However, this technique is quite challenging, and accurate structural information is mainly obtained with the isotopic substitution method (NDIS), which compares experimental data of samples with the same atomic composition but different isotopes for a particular element. Unfortunately, a rather limited number of isotopes are suitable for NDIS, as isotopes should have reasonably large differences in their scattering lengths. As a consequence, the coordination geometry of hydrogen atoms in the first hydration shell is usually poorly defined, and the aid of a new experimental technique may be essential to gain deeper insight into the structural properties of aqueous solutions. The Nd–H first-shell signals are quite strong and provide a detectable contribution to the total $\chi(k)$ signal up to about 11 $Å^{-1}$ (see Figure 5). The structural results for the Nd–H first-shell distances are listed in Table 1. Proof of the importance of including the hydrogen signal in the analysis of the EXAFS spectra of lanthanoid(III) aqueous solutions has been obtained by performing an additional fitting procedure on the EXAFS spectrum of solid $[Nd(H_2O)_9](CF_3SO_3)_3$ without including the hydrogen signals. The fitting procedure was applied both to the structural parameters associated with the Nd–O single- and multiple-scattering signals, and to the nonstructural and background parameters. Note that the E_0, S_0^2, and double-electron excitation parameters obtained from this minimization were equal, within the reported errors, to those determined from the previous analysis including the hydrogen contributions. The results of this minimization are shown in the upper panel of Figure 10, where the total theoretical signal, including the Nd–O first shell and the MS contributions, is compared with the experimental spectrum. Agreement between experimental and theoretical signals is not particularly good, especially in the k region below 9 $Å^{-1}$. The presence of an additional contribution that has not been included in the theoretical calculation is confirmed by the residual curve shown in the upper panel of Figure 10. The amplitude of this signal is quite large and, together with the noise of the experimental spectrum, the presence of a leading frequency can be identified clearly. This finding clearly demonstrates that the hydrogen atoms provide a detectable contribution to the XAFS spectra of lanthanoid(III) ions in aqueous solution, which must be taken into account to perform a complete analysis of the experimental data. It is interesting to observe the effect of omitting the hydrogen contribution on the refined values of the structural parameters. All the ion–O first-shell parameters determined from the minimization not including the H signals were found to be equal to those of Table 1, within the reported errors. Therefore, reliable structural information on the ion–H $g(r)$ can be obtained from the XAS technique, but exclusion of the hydrogen contribution does not significantly affect the

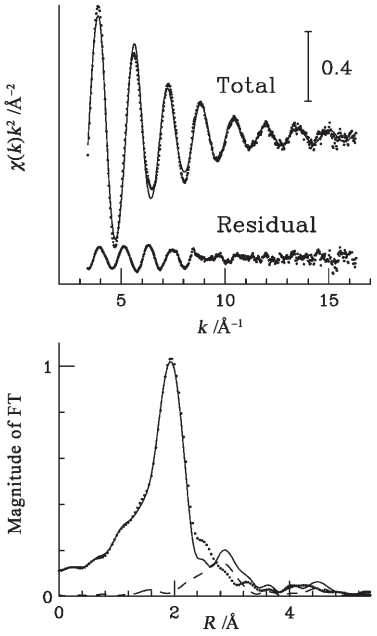

Figure 10. Top: comparisons between the EXAFS experimental spectrum of solid $[Nd(H_2O)_9](CF_3SO_3)_3$ at the K-edge and the theoretical signal not including the hydrogen contribution. Bottom: nonphase-shift-corrected Fourier transforms of the experimental data (dotted line), of the theoretical signal (full line) not including the ion–H signals, and of the residual curve (dashed line).

accuracy of the ion–O first-shell structural parameters obtained from the EXAFS data analysis. The FT of the theoretical, experimental, and residual signals of Figure 10 are shown in the lower panel. They were calculated in the same k range as the previous analysis, with no phase-shift corrections applied. The agreement between theoretical and experimental curves is not very good in the distance range between 2 and 3 Å. The peak at about 3 Å in the FT of the residual curve is clearly associated with the hydrogen-shell distribution, as no other structural contributions are present in this distance range.

Comparison of different lanthanoid(III) ions: A complete picture of the potential of XAS spectroscopy at the K-edge of lanthanoid(III) ions can be drawn by comparing the characteristics of the EXAFS spectra throughout the series. To this end, we carried out EXAFS data analysis of solid $[M(H_2O)_n](CF_3SO_3)_3$ [M = La, Eu (n = 9); M = Lu (n = 8.2]. All of the analyses started from the tricapped trigonal configuration determined by X-ray diffraction,[21,22] and used a two-shell model. The results of the minimization procedures are shown in Figure 11, while the structural parameters are listed in Table 2. It is interesting to compare the amplitude of the experimental $\chi(k)$ signals in the three cases. As expected, the core-hole effect is much more evident at higher energy. In particular, the low-k region of the lutetium spectrum is strongly damped as compared to that of lanthanum, due to both the core-hole and Debye–Waller effects. Moreover, the hydrogen contribution becomes much smaller at higher energies, and the MS effects make a negligible contribution in the case of the lutetium(III) ion. This is not surprising, as the short lifetime of the excited atomic state causes damping of the longer distance components of the EXAFS signal, and reduces the sensitivity of this technique to the more distant shells. Nevertheless, the ion–O first-shell parameters can be extracted from the experimental data with high accuracy, due also to the large k range that can be analyzed (see Table 2).

Table 2. First-shell structural parameters of solid lanthanum(III), europium(III), and lutetium(III) trifluoromethanesulfonate from EXAFS data analysis at the K-edge.

	N	R [Å]	σ^2 [Å^2]	β
La–O1	6.0(0.5)	2.560(0.009)	0.0070(0.0013)	0.5(0.6)
La–O2	3.0(0.8)	2.660(0.018)	0.0065(0.0022)	0.4(0.2)
La–H1	11.8(0.7)	3.25(0.03)	0.008(0.005)	1.0(0.5)
La–H2	6.0(0.8)	3.38(0.05)	0.006(0.006)	0.29(0.6)
Eu–O1	6.0(0.5)	2.433(0.009)	0.0064(0.0015)	0.6(0.2)
Eu–O2	3.0(0.9)	2.565(0.016)	0.0090(0.0034)	0.8(0.2)
Eu–H1	12.1(0.8)	3.14(0.03)	0.016(0.009)	0.4(0.5)
Eu–H2	6.0(0.9)	3.18(0.05)	0.006(0.006)	0.2(0.6)
Lu–O1	6.0(0.7)	2.317(0.009)	0.0058(0.0018)	0.2(0.2)
Lu–O2	3.0(0.9)	2.376(0.018)	0.0067(0.0055)	0.2(0.2)
Lu–H1	11.7(0.9)	3.11(0.09)	0.004(0.009)	0.9(0.5)
Lu–H2	6.1(0.9)	3.09(0.12)	0.004(0.009)	0.9(0.6)

Finally, we compare the amplitude of the O1-ion-O1 MS theoretical signals calculated on the basis of the tricapped trigonal geometry for some of the lanthanoid(III) ions at the L_3- and K-edges. The O-ion-O MS contributions are shown in the left and right panels of Figure 12 for the L_3- and K-edge data, respectively. Note that the amplitude of the three-body contributions is almost the same across the series at the L_3-edge, while it shows a dramatic drop at the K-edge. As a result, if one is mainly interested in the angular distribution of the first-shell cluster, analysis of the L_3-edges is better suited.

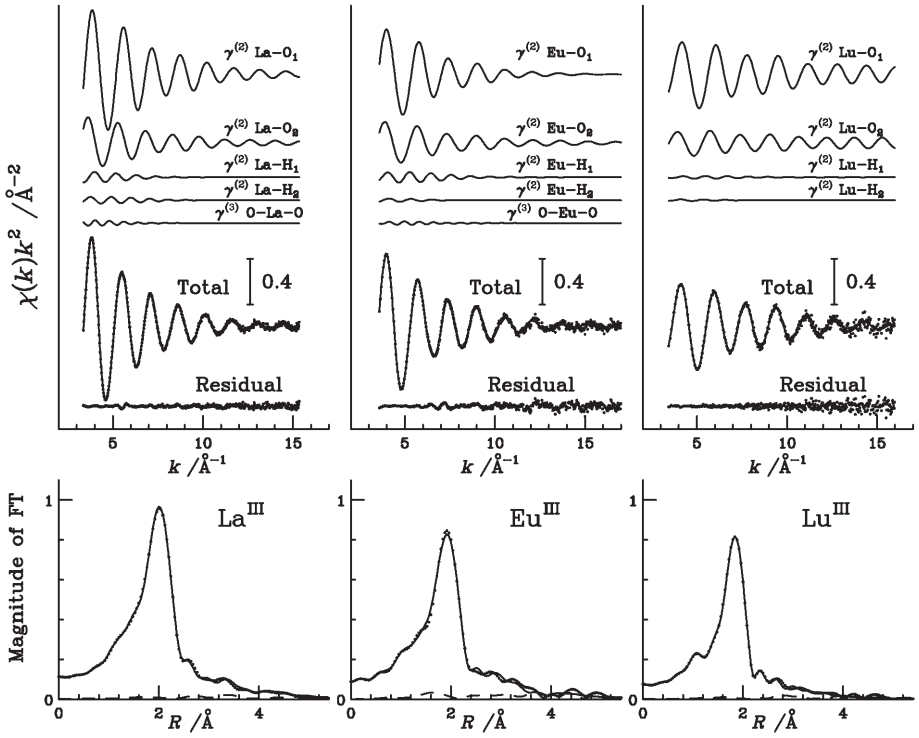

Figure 11. Fit of the K-edge EXAFS spectra of solid $[La(H_2O)_9](CF_3SO_3)_3$ (left), $[Eu(H_2O)_9](CF_3SO_3)_3$ (middle), and $[Lu(H_2O)_9](CF_3SO_3)_3$ (right). From top to bottom in each panel, the following curves are reported: the ion–O first-shell signals, the ion–H first-shell signals, the O1-ion-O1 three-body signals, the total theoretical signals compared with the experimental spectrum, and the residual curves. The lower panels show the nonphase-shift-corrected Fourier transforms of the experimental data (dotted line), of the total theoretical signals (full line), and of the residual curves (dashed-dotted line).

Conclusions

We have measured XAS spectra at the K-edge of lanthanoid(III) ions in aqueous

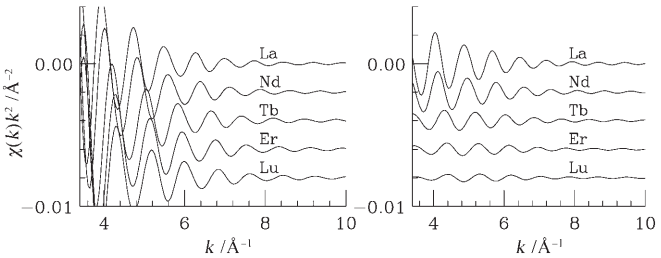

Figure 12. Theoretical O1-ion-O1 three-body signals of different lanthanoid(III) ions calculated for the L_3-edge (left panel) and K-edge (right panel).

solution in the energy range 38–65 keV and demonstrated the feasibility and the power of high-energy EXAFS. The effect of core-hole lifetime broadening, though apparent, is manageable if high-quality data are collected over the large k range accessible for heavy-element K-edges. Analysis of the K-edge EXAFS data provides more accurate structural results as compared to the L_3-edge, given a well-defined structure. This is due both to the smaller influence of the double-electron excitations and to the wider available k range. From the analysis of a single EXAFS spectrum it is not possible to unambiguously determine the first-shell coordination number if the studied complex is not highly symmetric. However, the distance trend obtained from the analysis of the K-edge data can be successfully used to elucidate geometrical change in the hydration structure throughout the lanthanoid series. By using this approach a clear picture of the hydration structure of lanthanoid(III) ions has been obtained, and these results are reported in the following paper.[9]

The results of this investigation pave the way for the use of K-edge absorption spectroscopy for structural investigations of systems containing heavy elements.

Experimental Section

EXAFS data collection: Aqueous solutions of the trivalent lanthanoids were made by dissolving weighed amounts of hydrated trifluoromethanesulfonates $[Ln(H_2O)_n](CF_3SO_3)_3$ (Ln = La, Pr, Nd, Sm, Eu, Gd, Tb, Dy, Ho, Er, Tm, Yb, Lu) in freshly distilled water. The concentration of the samples was 0.2 M and the solutions were acidified to about pH 1 by adding trifluoromethanesulfonic acid. The data were collected at ESRF on the bending magnet X-ray absorption spectroscopy beamline BM29[25] in transmission geometry. The storage ring was operating in 16-bunch mode with a typical current of 80 mA after refill. The K-edge spectra were collected by using an Si(511) double-crystal monochromator with the second crystal detuned by 20% for harmonic rejection. The aqueous solutions were kept in cells with Kapton film windows and Teflon spacers ranging from 2 to 3 cm depending on the sample. Solid $[Ln(H_2O)_n](CF_3SO_3)_3$ [Ln = La, Nd, Eu, Gd, Tb, Dy ($n=9$); Ho ($n=8.91$); Er ($n=8.96$); Tm ($n=8.8$); Yb ($n=8.7$); and Lu ($n=8.2$] were diluted with boron nitride to give an absorption change over the edge of about one logarithmic unit. The L_3- and L_1-edge spectra of solid $[Nd(H_2O)_9](CF_3SO_3)_3$ were recorded by using an Si(311) Si(511) double-crystal monochromator with the second crystal detuned by 50% for harmonic rejection. The L_1-edge spectrum of neodymium(III) in aqueous solution was collected by using the same experimental setup, but the sample was kept in a cell with 500 μm Teflon spacer.

EXAFS data analysis: The EXAFS data were analyzed with the GNXAS program, which has proved to give reliable structural information also in the high-energy domain.[23,26] This method is based on the theoretical calculation of the EXAFS signal and a subsequent refinement of the structural parameters. In this approach, interpretation of the experimental data is based on the decomposition of the $\chi(k)$ signal into a summation over n-body distribution functions, calculated by means of multiple-scattering (MS) theory.

The theoretical signal $\chi(k)$ is related to the experimental absorption coefficient $\alpha(k)$ through the relation $\alpha(k)=J\sigma_0(k)S_0^2[1+S_0^2\chi(k)]+\beta(k)$, where $\sigma_0(k)$ is the atomic cross section, J the edge jump, S_0^2 provides a uniform reduction of the signal and is associated with many-body corrections to the one-electron cross section, and $\beta(k)$ is the background function, which accounts for further absorbing processes. Multielectron excitation channels are accounted for by modeling the $\beta(k)$ function as the sum of a smooth polynomial spline and step-shaped functions.

In the present study the lanthanoid(III)–oxygen first coordination shells were modeled with gammalike functions which depend on four parameters, namely, the coordination number N, the average distance R, the distance variance σ^2, and the skewness β. The β value is related to the third cumulant C_3 of the distance distribution through the relation $C_3=\sigma^3\beta$, and R is its first moment. The three-body distributions associated with the O-Ln-O configurations were also considered, and the structural parameters were the two bond lengths, the intervening angle θ, and the six covariance matrix elements. Additional nonstructural parameters were minimized, namely, E_0 (core ionization threshold energy) and S_0^2.

Least-squares fits of the EXAFS raw experimental data were performed by minimizing a residual function of the type [Eq. (1)]

$$R_i(\{\lambda\}) = \sum_{i=1}^{N} \frac{[\alpha_{exp}(E_i)-\alpha_{mod}(E_i;\lambda_1, \lambda_2, \ldots, \lambda_p)]^2}{\sigma_i^2} \quad (1)$$

where N is the number of experimental points E_i, $\{\lambda\}=(\lambda_1, \lambda_2, \ldots, \lambda_p)$ are the p parameters to be refined, and σ_i^2 is the noise variance associated with each experimental point $\alpha_{exp}(E_i)$.[23] Phase shifts were calculated by using muffin-tin potentials and advanced models for the exchange-correlation self-energy (Hedin–Lundqvist).[27]

Acknowledgements

We acknowledge the European Synchrotron Radiation Facility for provision of synchrotron radiation facilities and we thank Dr. Michael Borowski for assistance in using beamline BM29. The support from the Swedish Research Council is acknowledged (I.P.).

[1] A. Kodre, I. Arčon, M. Hribar, M. Stuhec, F. Villain, W. Drube, L. Tröger, *Physica B+C* **1995**, *208*, 379–380.
[2] J. A. Solera, J. García, M. G. Proietti, *Phys. Rev. B* **1995**, *208*, 2678–2686.
[3] P. D'Angelo, N. V. Pavel, D. Roccatano, H.-F. Nolting, *Phys. Rev. B* **1996**, *54*, 12129–12138.
[4] M. Borowski, D. T. Bowron, S. De Panfilis, *J. Synchrotron Radiat.* **1999**, *6*, 179–181.
[5] a) P. D'Angelo, N. V. Pavel, M. Borowski, *J. Synchrotron Radiat.* **2001**, *8*, 666–668; b) J. M. Cole, R. Newport, D. Bowron, R. F. Pettifer, G. Mountjoy, T. Brennan, G. A. Saunders, *J. Phys. Condens. Matter* **2001**, *13*, 6659–6674.
[6] a) J. Chaboy, E. Cotallo, S. Quartieri, F. Boscherini, *J. Synchrotron Radiat.* **2002**, *9*, 86–89; b) F. d'Acapito, S. Mobilio, L. Santos, M. Almeida Rui, *Appl. Phys. Lett.* **2001**, *78*, 2676–2678; c) S. Quartieri, F. Boscherini, J. Chaboy, M. C. Dalconi, R. Oberti, A. Zanetti, *Phys. Chem. Miner.* **2002**, *29*, 495–502; d) S. Quartieri, M. C. Dalconi, F.

Boscherini, R. Oberti, F. D'Acapito, *Phys. Chem. Miner.* **2004**, *31*, 162–167.
[7] Y. Nishihata, O. Kamishima, Y. Kubozono, H. Maeda, S. Emura, *J. Synchrotron Radiat.* **1998**, *5*, 1007–1009.
[8] a) Y. Nishihata, S. Emura, H. Maeda, Y. Kubozono, M. Harada, T. Uruga, H. Tanida, Y. Yoneda, J. Mizuki, T. Emoto, *J. Synchrotron Radiat.* **1999**, *6*, 149–151; b) Y. Nishihata, J. Mizuki, S. Emura, T. Uruga, *J. Synchrotron Radiat.* **2001**, *8*, 294–296; c) T. Yamamoto, T. Tanaka, T. Matsuyama, T. Funabiki, S. Yoshida, *J. Synchrotron Radiat.* **2001**, *8*, 634–636.
[9] I. Persson, P. D'Angelo, S. De Panfilis, M. Sandström, L. Eriksson, *Chem. Eur. J.* **2008**, *14*, DOI: 10.1002/chem.200701281..
[10] a) A. Abbasi, E. Damian Risberg, L. Eriksson, J. Mink, I. Persson, M. Sandström, Y. V. Sidorov, M. Y. Skripkin, A.-S. Ullström, *Inorg. Chem.* **2007**, *46*, 7731–7741; b) I. Persson, E. Damian Risberg, P. D'Angelo, S. De Panfilis, M. Sandström, A. Abbasi, *Inorg. Chem.* **2007**, *46*, 7742–7748.
[11] D. Lundberg, L. Eriksson, I. Persson, P. D'Angelo, S. De Panfilis in D. Lundberg, "The Coordination Chemistry of Solvated Metal Ions in DMPU—A Study of a Space-Demanding Solvent", Doctoral Thesis No. 2006:23, Faculty of Natural Resources and Agricultural Sciences, Swedish University of Agricultural Sciences, Uppsala 2006.
[12] M. O. Krause, J. H. Oliver, *J. Phys. Chem. Ref. Data* **1979**, *8*, 329–338.
[13] A. Filipponi, *J. Phys. B* **2000**, *33*, 2835–2846.
[14] T. Yamaguchi, M. Nomura, H. Wakita, H. Ohtaki, *J. Chem. Phys.* **1988**, *89*, 5153–5159.
[15] S. Bénazeth, J. Purans, M.-C. Chalbot, M. Kim Nguyen-van-Duong, L. Nicolas, F. Keller, A. Gaudemer, *Inorg. Chem.* **1998**, *37*, 3667–3674.
[16] P. Lindqvist-Reis, K. Lamble, S. Pattanik, I. Persson, M. Sandström, *J. Phys. Chem. B* **2000**, *104*, 402–408.
[17] J. Chaboy, J. García, A. Marcelli, M. R. Ruiz-López, *Chem. Phys. Lett.* **1990**, *174*, 389–395.
[18] J. Chaboy, T. A. Tyson, *Phys. Rev. B* **1994**, *49*, 5869–5875.
[19] J. Chaboy, A. Marcelli, T. A. Tyson, *Phys. Rev. B* **1994**, *49*, 11652–11661.
[20] P. D'Angelo, A. Di Cicco, A. Filipponi, N. V. Pavel, *Phys. Rev. A* **1993**, *47*, 2055–2063.
[21] A. Chatterjee, E. N. Maslen, K. J. Watson, *Acta Crystallogr. Sect. A* **1988**, *44*, 381–386.
[22] C. O. P. Santos, E. E. Castellano, L. C. Machado, G. Vicentini, *Inorg. Chim. Acta* **1985**, *110*, 83–86.
[23] A. Filipponi, A. Di Cicco, *Phys. Rev. B* **1995**, *52*, 15135–15149.
[24] P. D'Angelo, V. Barone, G. Chillemi, N. Sanna, W. Meyer-Klaucke, N. V. Pavel, *J. Am. Chem. Soc.* **2002**, *124*, 1958–1967.
[25] A. Filipponi, M. Borowski, D. T. Bowron, S. Ansell, S. De Panfilis, A. Di Cicco, J.-P. Itiè, *Rev. Sci. Instrum.* **2000**, *71*, 2422–2432.
[26] A. Filipponi, A. Di Cicco, C. R. Natoli, *Phys. Rev. B* **1995**, *52*, 15122–15134.
[27] L. Hedin, B. I. Lundqvist, *J. Phys. C* **1971**, *4*, 2064–2083.

Received: August 17, 2007
Revised: November 19, 2007
Published online: February 1, 2008

